# Coupling light into a slow-light photonic-crystal waveguide from a free-space normally-incident beam

Philippe Hamel, Patricio Grinberg, Christophe Sauvan, Philippe Lalanne, Alexandre Baron, Alejandro M. Yacomotti, Isabelle Sagnes, Fabrice Raineri, Kamel Bencheikh, Juan Ariel Levenson

# Coupling light into a slow-light photonic-crystal waveguide from a free-space normally-incident beam

P. Hamel,[1,*] P. Grinberg,[1] C. Sauvan,[2] P. Lalanne,[2]
A. Baron,[2] A.M. Yacomotti,[1] I. Sagnes,[1] F. Raineri,[1] K. Bencheikh,[1] and J.A. Levenson[1]

[1]*Laboratoire de Photonique et de Nanostructures (CNRS UPR20), Route de Nozay, 91460 Marcoussis, France*
[2]*Laboratoire Photonique Numérique et Nanosciences, Institut d'Optique Graduate School, Université Bordeaux, CNRS, 33405 Talence, France*
*[*]philippe.hamel@lpn.cnrs.fr*

**Abstract:** We present a coupler design allowing normally-incident light coupling from free-space into a monomode photonic crystal waveguide operating in the slow-light regime. Numerical three-dimensional calculations show that extraction efficiencies as high as 80% can be achieved for very large group indices up to 100. We demonstrate experimentally the device feasibility by coupling and extracting light from a photonic crystal waveguide over a large group-index range (from 10 to 60). The measurements are in good agreement with theoretical predictions. We also study numerically the impact of various geometrical parameters on the coupler performances.

©2013 Optical Society of America

OCIS codes: (130.5296) Photonic crystal waveguides; (230.7400) Waveguides, slab; (220.4241) Nanostructure fabrication.

## References and links

1. M. Notomi, K. Yamada, A. Shinya, J. Takahashi, C. Takahashi, and I. Yokohama, "Extremely Large Group-Velocity Dispersion of Line-Defect Waveguides in Photonic Crystal Slabs," Phys. Rev. Lett. **87**(25), 253902 (2001).
2. T. Baba, "Slow light in photonic crystals," Nat. Photonics **2**(8), 465–473 (2008).
3. T. F. Krauss, "Why do we need slow light?" Nat. Photonics **2**(8), 448–450 (2008).
4. C. Monat, B. Corcoran, M. Ebnali-Heidari, C. Grillet, B. J. Eggleton, T. P. White, L. O'Faolain, and T. F. Krauss, "Slow light enhancement of nonlinear effects in silicon engineered photonic crystal waveguides," Opt. Express **17**(4), 2944–2953 (2009).
5. K. Inoue, H. Oda, N. Ikeda, and K. Asakawa, "Enhanced third-order nonlinear effects in slow-light photonic-crystal slab waveguides of line-defect," Opt. Express **17**(9), 7206–7216 (2009).
6. J. P. Hugonin, P. Lalanne, T. P. White, and T. F. Krauss, "Coupling into slow-mode photonic crystal waveguides," Opt. Lett. **32**(18), 2638–2640 (2007).
7. Y. A. Vlasov and S. J. McNab, "Coupling into the slow light mode in slab-type photonic crystal waveguides," Opt. Lett. **31**(1), 50–52 (2006).
8. P. Barclay, K. Srinivasan, and O. Painter, "Design of photonic crystal waveguides for evanescent coupling to optical fiber tapers and integration with high- Q cavities," J. Opt. Soc. Am. B **20**(11), 2274 (2003).
9. M. W. Lee, C. Grillet, C. G. Poulton, C. Monat, C. L. C. Smith, E. Mägi, D. Freeman, S. Madden, B. Luther-Davies, and B. J. Eggleton, "Characterizing photonic crystal waveguides with an expanded k-space evanescent coupling technique," Opt. Express **16**(18), 13800–13808 (2008).
10. Q. V. Tran, S. Combrié, P. Colman, and A. De Rossi, "Photonic crystal membrane waveguides with low insertion losses," Appl. Phys. Lett. **95**(6), 061105 (2009).
11. S. McNab, N. Moll, and Y. Vlasov, "Ultra-low loss photonic integrated circuit with membrane-type photonic crystal waveguides," Opt. Express **11**(22), 2927–2939 (2003).
12. M. Notomi, A. Shinya, S. Mitsugi, E. Kuramochi, and H. Ryu, "Waveguides, resonators and their coupled elements in photonic crystal slabs," Opt. Express **12**(8), 1551–1561 (2004).
13. D. Taillaert, W. Bogaerts, P. Bienstman, T. F. Krauss, P. Van Daele, I. Moerman, S. Verstuyft, K. De Mesel, and R. Baets, "An out-of-plane grating coupler for efficient butt-coupling between compact planar waveguides and single-mode fibers," IEEE J. Quantum Electron. **38**(7), 949–955 (2002).

14. F. Van Laere, G. Roelkens, M. Ayre, J. Schrauwen, D. Taillaert, D. Van Thourhout, T. F. Krauss, and R. Baets, "Compact and highly efficient grating couplers between optical fiber and nanophotonic waveguides," J. Lightwave Technol. **25**(1), 151–156 (2007).
15. N. Le Thomas, R. Houdré, L. Frandsen, J. Fage-Pedersen, A. Lavrinenko, and P. Borel, "Grating-assisted superresolution of slow waves in Fourier space," Phys. Rev. B **76**(3), 035103 (2007).
16. C.-C. Tsai, J. Mower, and D. Englund, "Directional free-space coupling from photonic crystal waveguides," Opt. Express **19**(21), 20586–20596 (2011).
17. E. Kuramochi, M. Notomi, S. Hughes, A. Shinya, T. Watanabe, and L. Ramunno, "Disorder-induced scattering loss of line-defect waveguides in photonic crystal slabs," Phys. Rev. B **72**(16), 161318 (2005).
18. S. Mazoyer, P. Lalanne, J. C. Rodier, J. P. Hugonin, M. Spasenović, L. Kuipers, D. M. Beggs, and T. F. Krauss, "Statistical fluctuations of transmission in slow light photonic-crystal waveguides," Opt. Express **18**(14), 14654–14663 (2010).
19. N.-V.-Q. Tran, S. Combrié, P. Colman, A. De Rossi, and T. Mei, "Vertical high emission in photonic crystal nanocavities by band-folding design," Phys. Rev. B **82**(7), 075120 (2010).
20. S. Haddadi, L. Le-Gratiet, I. Sagnes, F. Raineri, A. Bazin, K. Bencheikh, J. A. Levenson, and A. M. Yacomotti, "High quality beaming and efficient free-space coupling in L3 photonic crystal active nanocavities," Opt. Express **20**(17), 18876–18886 (2012).
21. T. Tamir and S. T. Peng, "Analysis and design of grating couplers," Appl. Phys., A Mater. Sci. Process. **14**, 235–254 (1977).
22. P. Lalanne, C. Sauvan, and J. P. Hugonin, "Photon confinement in photonic crystal nanocavities," Laser Photon. Rev. **2**(6), 514–526 (2008).
23. P. Lalanne, "Electromagnetic analysis of photonic crystal waveguides operating above the light cone," IEEE J. Quantum Electron. **38**(7), 800–804 (2002).
24. G. Lecamp, J. P. Hugonin, and P. Lalanne, "Theoretical and computational concepts for periodic optical waveguides," Opt. Express **15**(18), 11042–11060 (2007).
25. J. P. Hugonin and P. Lalanne, "Perfectly matched layers as nonlinear coordinate transforms: a generalized formalization," J. Opt. Soc. Am. A **22**(9), 1844–1849 (2005).
26. M. G. Moharam, E. B. Grann, D. A. Pommet, and T. K. Gaylord, "Formulation for stable and efficient implementation of the rigorous coupled-wave analysis of binary gratings," J. Opt. Soc. Am. A **12**(5), 1068–1076 (1995).
27. L. Li, "New formulation of the Fourier modal method for crossed surface-relief gratings," J. Opt. Soc. Am. A **14**(10), 2758–2767 (1997).
28. T. J. Karle, Y. Halioua, F. Raineri, P. Monnier, R. Braive, L. Le Gratiet, G. Beaudoin, I. Sagnes, G. Roelkens, F. van Laere, D. Van Thourhout, and R. Raj, "Heterogeneous integration and precise alignment of InP-based photonic crystal lasers to complementary metal-oxide semiconductor fabricated silicon-on-insulator wire waveguides," J. Appl. Phys. **107**(6), 063103 (2010).
29. S. Mazoyer, "Lumière lente dans les guides à cristaux photoniques réels," PhD thesis, Université Paris Sud, *http://hal-iogs.archives-ouvertes.fr/docs/00/65/07/43/PDF/Total_final.pdf*
30. S. Combrié, E. Weidner, A. DeRossi, S. Bansropun, S. Cassette, A. Talneau, and H. Benisty, "Detailed analysis by Fabry-Perot method of slab photonic crystal line-defect waveguides and cavities in aluminium-free material system," Opt. Express **14**(16), 7353–7361 (2006).

## 1. Introduction

Photonic crystal waveguides (PhCWs) have been a research focus in photonics for several years and have led to a wide range of applications notably in the domain of slow light [1–3] and enhanced non-linear effects [4,5]. While current studies still investigate the wide range of engineering possibilities offered by photonic crystal structures, a parallel key objective is to develop efficient methods for coupling/extracting light in/from PhCWs. This issue remains indeed challenging since the typical waveguide cross-sections (<1µm width and <500nm thickness) make it difficult to couple light in from any other system (fibered or free-space) usually exhibiting a large mode-profile mismatch. Additional difficulties are encountered when coupling into slow-light PhCWs because of the group-velocity mismatch resulting in a strong reflection at the interface between the injection medium and the PhCW.

To address these issues, various types of systems have already demonstrated their efficiency for coupling "standard" waveguides (ridge or PhCW in "non-slow-light" regime) with slow-light PhCWs [6,7]. In addition, many solutions have also been proposed to directly couple light into PhCWs both from waveguides and free-space. Tapered-fiber evanescent couplers [8,9], mode adapters [10–12] and grating based couplers [13,14] have proven to be very efficient by exhibiting typical coupling efficiency values up to 60%.

However, these solutions typically require both a long on-chip access system to couple light into a slow-light PhCW and/or major modifications of their original design. This appears to be problematic when the presence of an absorptive medium (quantum dots, quantum wells) is needed for some specific applications. Indeed, a strong absorption requires that the whole system (couplers + PhCW) remains short to avoid losing power through transmission.

After Le Thomas and associates [15] had proposed an efficient way to access modes below the light line by using one dimensional grating Tsai and associates [16] reported a method allowing direct vertical coupling to a PhCW. A Finite Difference Time Domain (FDTD) analysis was performed to calculate local PhC lattice modifications that could generate a vertical coupler. Numerical calculations showed an extraction angle restrained to low values ($< 20°$) and a good coupling efficiency ($\approx 60\%$) from the PhCW fundamental mode to a Gaussian beam. However, to our knowledge, no experimental demonstration of such method has been reported. Furthermore, the aforementioned study mainly focuses on a single frequency at the band edge, which corresponds to extremely high group index values that are liable for strong disorder-induced losses [17,18].

Independently of these recent studies focused on waveguides, the concept of band-folding has been proposed to achieve beaming in PhC cavities [19]. Its purpose is to optimize the emission profile through a periodic modification of the design. Typical results show a divergence of the vertical emission widely reduced ($<30°$) and consequently a more efficient injection/collection through the use of standard optics [20].

We propose here to transpose band-folding concepts to waveguides in order to achieve a vertical coupling in and out the PhCW directly from free-space. We show that it can be performed on very short waveguides (down to tens of μm) and neither cleaving nor major design modification is required. By adding a local super-periodicity to the PhC lattice, we design in Section 2 a diffractive element that is used both as a vertical coupler and extractor from the waveguide. We show experimentally in Section 3 that the proposed device allows coupling and extracting slow light nearly perpendicular to the waveguide over a broad group-index range ($10 < n_g < 60$). Finally, in Section 4, we analyze numerically the impact of various geometrical parameters on the coupler performance. In particular, we show how the group-index range where the extraction efficiency is high can be changed.

## 2. Design of the coupler

The coupler has been designed for coupling/extracting light perpendicularly to the PhCW for a group index of $n_g = 20$ ($\lambda = 1.55$ μm). The PhCW, sketched in Fig. 1(a), is a usual W1 waveguide formed by removing one row of holes in a photonic crystal (with a lattice period $a = 430$ nm and a hole radius $r = 110$ nm). We have first calculated the effective index (normalized propagation constant) $n_0 = 2.15$ of the TE-like fundamental Bloch mode supported by the W1 waveguide for this specific wavelength. Then, as for classical grating-coupler designs [21], we assume that the W1 waveguide is perturbed by a periodic modulation with a periodicity $\Lambda$ shown by the small holes in Fig. 1(b).

This perturbation acts as a grating coupler with an out-of-plane leakage at normal incidence provided that the phase-matching condition

$$k_0 n_0 - mK = 0 \tag{1}$$

is satisfied, where $k_0 = 2\pi/\lambda$, $K = 2\pi/\Lambda$ and $m$ is an integer. This phase-matching condition imposes that the additional period $\Lambda$ folds the dispersion curve of the Bloch mode of the W1 waveguide above the light line around $k = 0$. Equation (1) is valid provided that one neglects the effective-index change induced by the weak periodic modulation [21]. For $m = 1, 2$ we find $\Lambda = 0.68$ μm ($\approx 1.6a$) and $\Lambda = 1.35$ μm ($\approx 3.2a$). The perturbed waveguide in Fig. 1(b) is no longer periodic (except for very long super-periods $\Lambda$) because $\Lambda$ and $a$ are not commensurate in general. Although the perturbed waveguide of Fig. 1(b) is likely extracting

light vertically, we have deliberately chosen to opt for a full-periodic coupler design by changing the PhC period along the propagation direction in order to render $\Lambda$ and the new period $a_c$ commensurate. In comparison to the case $m = 1$, the $m = 2$ case is more favorable since a periodicity $\Lambda \approx 3.2a$ requires only a slight increase of the longitudinal period, which becomes $a_c = \Lambda/3 = a + 30$ nm $= 460$ nm. The resulting periodic coupler (super-period $\Lambda = 3a_c$) is shown in Fig. 1(c).



**(a)**
W1 waveguide

**(b)**
Perturbed
coupler

**(c)**
Perturbed
periodic coupler

**(d)**
Heterostructure
coupler
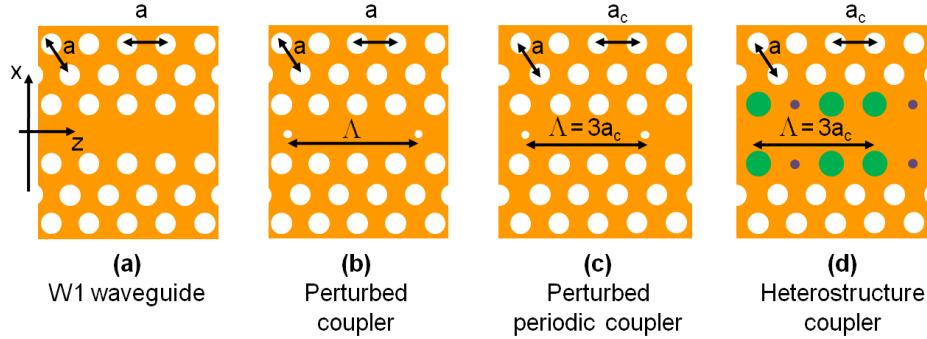
Fig. 1. Successive steps of the design process. The objective is to realize a periodic diffractive element compatible with the PhC periodicity and able to couple/extract light in/from the PhCW shown in (a). The waveguide is formed by removing one row of holes in a triangular lattice (period $a = 430$ nm) of air holes (radius $r = 110$ nm) etched into an InP membrane (refractive index $n = 3.16$ and thickness $h = 265$ nm). (b) Adding a periodic perturbation (super-period $\Lambda$) to the W1 waveguide creates in general an aperiodic coupler because both periods $a$ and $\Lambda$ are not commensurate. (c) A periodic coupler is obtained by increasing the longitudinal period of the PhC, $a_c = a + 30$ nm $= 460$ nm, in order to render $\Lambda$ and the new period $a_c$ commensurate, $\Lambda = 3a_c$. (d) We have chosen to keep the holes position unchanged and to create the periodic perturbation by increasing and decreasing the radius of the two inner rows of holes ($r_c = r \pm \Delta r$). We obtain a heterostructure coupler with a super-period $\Lambda = 3a_c$.

Finally, in order to minimize the impedance-mismatch between the guided Bloch mode of the W1 waveguide and the leaky Bloch mode of the coupler [22], we have decided to avoid etching the central part of the waveguide and to use a heterostructure geometry in which solely the two inner rows of holes are modified, see Fig. 1(d). To keep the average effective index almost constant in order to satisfy the phase matching condition of Eq. (1), we increase the radius of some holes and decrease that of others. The radius increment is denoted by $\Delta r$. Figure 1(d) shows the resulting heterostucture coupler with a super-period $\Lambda = 3a_c$.

The increase of the PhC longitudinal period inside the coupler ($a_c > a$) changes the value of the effective index that has to be folded above the light cone and Eq. (1) is not exactly satisfied. We have optimized the parameter $\Delta r$ to take into account this effect and to guaranty coupling/extracting at nearly normal incidence for $n_g = 20$ ($\lambda = 1.55$ µm). We have calculated the leaky mode supported by the coupler in Fig. 1(d) for different values of $\Delta r$ by using a Bloch mode solver able to analyze leaky Bloch modes of PhCWs operating above the clad light cone [23]. Table 1 summarizes the main properties of the leaky Bloch mode supported by the heterostructure coupler for $\Delta r = 35$ nm. The imaginary part of the effective index Im($n_{eff}$) is a measure of the damping rate of the leaky mode inside the coupler in the absence of absorption, and the real part folded in the first Brillouin zone gives the angle θ between the normal to the PhC membrane and the main direction of the diffracted light, θ = arcsin[Re($n_{eff}$) − $m\lambda/\Lambda$]. We have also performed simulations by varying the periodicity ($a = 430 \pm 10$ nm) and the hole radius of the PhC ($r = 110 \pm 20$ nm), using exactly the same design for the heterostructure coupler ($a_c = a + 30$ nm and $\Delta r = 35$ nm). The simulations have shown that the design is robust to fabrication imperfections, which has been confirmed by experimental results not reported hereafter.

**Table 1. Characteristics of the leaky Bloch mode supported by the heterostructure coupler shown in Fig. 1(d) with $a$ = 430 nm, $a_\text{c}$ = 460 nm, $r$ = 110 nm and $\Delta r$ = 35 nm.**

| Wavelength (µm) | Group index $n_\text{g}$ of the W1 waveguide | Effective index $n_\text{eff}$ of the coupler | Angle θ (°)[a] |
|---|---|---|---|
| 1.507 | 5 | 2.3186 + i0.0013 | 7.73 |
| 1.538 | 10 | 2.2461 + i0.0008 | 0.95 |
| 1.546 | 15 | 2.2394 + i0.0310 | −0.05 |
| 1.550 | 20 | 2.2439 + i0.0289 | −0.12 |
| 1.552 | 25 | 2.2453 + i0.0201 | −0.24 |
| 1.554 | 30 | 2.2378 + i0.0074 | −0.81 |
| 1.558 | 50 | 2.2109 + i0.0036 | −2.69 |
| 1.560 | 80 | 2.2000 + i0.0034 | −3.49 |

[a]The extraction angle θ is deduced from the real part of the effective index $n_\text{eff}$ of the leaky Bloch mode supported by the coupler, $\theta = \arcsin[\mathrm{Re}(n_\text{eff}) - m\lambda/\Lambda]$.

In order to evaluate the coupler performance, we have solved the scattering problem shown in Fig. 2(a), where the fundamental Bloch mode of the W1 waveguide is incident onto a coupler section with a finite length $L_\text{c} = N\Lambda$. The modal reflection $R$ corresponds to the *unwanted* backreflection and $T$ is the modal transmission due to the finite length of the coupler. The out-of-plane losses $O = 1 - R - T$ correspond exactly to the total amount of light that is extracted by the coupler. We therefore denote hereafter this quantity as the extraction efficiency of the coupler. The losses $O$ are also linked by reciprocity to the inverse process, the coupling from free-space to the PhCW, but we emphasize that $O$ is not directly the coupling efficiency. Since the structure is symmetric in the vertical direction, half of the energy is decoupled above the PhC membrane while the other half is decoupled below.

To calculate the scattering coefficients $R$ and $T$, one should be able to numerically handle outgoing-wave conditions in periodic waveguides. The Bloch-mode method that we use hereafter has been described in a previous work [24] for the general case of light propagation and light emission in three-dimensional (3D) periodic waveguides and in stacks of them. In brief, it operates in the frequency domain and relies on an analytical integration of Maxwell's equations along the longitudinal $z$-direction and on a supercell approach in the two transverse $x$- and $y$-directions. In these directions, Perfectly-Matched-Layers implemented as nonlinear coordinate transforms [25] are used to carefully handle out-of-plane far-field radiation in the clad. The numerical sampling in the transverse directions is performed in the Fourier space using truncated Fourier series. The approach directly relies on methods developed in the 90's for grating analysis [26,27]. The numerical results are obtained for truncation ranks $m_\text{x} = 25$ and $m_\text{y} = 14$, which implies that a total number of $M = (2m_\text{x} + 1) \times (2m_\text{y} + 1) = 1479$ Fourier coefficients are retained in the calculation. Indeed, the accuracy of the computational results increases as $M$ increases, but calculations performed for larger $M$ have revealed that the truncation error has no influence on the discussion and on the conclusions.

Figure 2 summarizes the main results for the coupler of Fig. 1(d) with $\Delta r$ = 35 nm. Note that this value corresponds to a significant perturbation $\Delta r/r$ = 32%. Figure 2(b) shows the dispersion curves of the two Bloch modes of importance in the structure. The guided Bloch mode supported by the W1 waveguide that is used as the incident mode is shown with the dashed line. It lies below the light cone (thin line) and has a cutoff wavelength where $n_\text{g} \rightarrow \infty$, $\lambda_\text{g}$ = 1.561 µm. The Bloch mode supported by the coupler is leaky; it is coupled to the continuum of radiative plane waves and its dispersion curve (solid line) lies above the light cone. It is important to note that the coupler mode possesses a band-gap at $k = 0$ around the target wavelength of the design ($\lambda$ = 1.55 µm and $n_\text{g}$ = 20) because of a coupling to the counter-propagating mode through the super-period $\Lambda$. The coupler thus acts as a leaky Bragg

mirror with a large reflection $R > 90\%$ inside the band-gap ($1.538 < \lambda < 1.552$ µm and $10 < n_g < 25$), as evidenced by the dashed blue line in Fig. 2(c) that shows the coupler reflection for $N = 30$ super-periods. As a consequence, the out-of-plane losses $O = 1 - R - T$ are low (see the solid red curve) and the coupling/extracting efficiencies are expected to be small in this spectral region. Outside the band-gap, the reflection decreases rapidly below 20% and the out-of-plane losses become significant. Both $R$ and $O$ present some oscillations, whose physical origin is the same as in the case of a usual Bragg mirror; they are Fabry-Perot fringes due to the bouncing of the leaky Bloch mode inside the finite-size coupler.
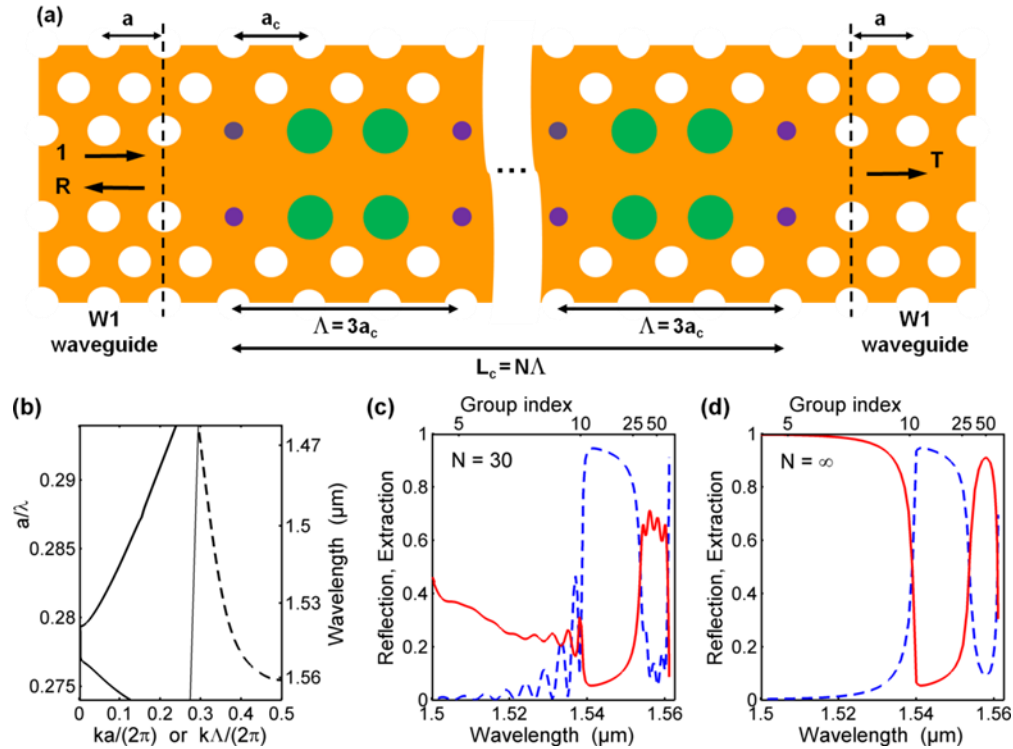


Fig. 2. Coupler performance. (a) The heterostructure coupler shown in Fig. 1(d) with $\Delta r = 35$ nm is inserted between two semi-infinite W1 waveguides. The coupler has a finite length $L_c = N\Lambda$ and its performance can be quantified by the reflection $R$, the transmission $T$ and the extraction efficiency $O = 1 - R - T$. (b) Dispersion curves of the guided Bloch mode of the W1 waveguide (dashed line) and of the leaky Bloch mode of the coupler (solid line). The latter lies above the light line (thin solid line). The guided Bloch mode of the W1 waveguide is used as the incident mode in the scattering problem in (a). Its cutoff wavelength where $n_g \to \infty$ is $\lambda_g \approx 1.561$ µm. (c) Reflection $R$ (dashed blue line) and extraction $O$ (solid red line) as a function of the wavelength for $N = 30$. (d) Same quantities for a semi-infinite coupler ($N = \infty$ and $O = 1 - R$ since $T = 0$). Large extraction efficiencies can be obtained around $n_g = 50$.

For large values of the incident group index, because of the group-velocity mismatch between the two Bloch modes, the reflection tends towards unity and no light can be coupled in/decoupled from the W1 waveguide [6,7]. The striking property of the designed structure is that this drop of the extraction efficiency appears only for very large group-index values of $n_g > 100$ (in a very narrow spectral window around 1.56 µm). As a result, even for group indices as large as $n_g = 50$, the extraction efficiency reaches 65% with a coupler made of $N = 30$ super-periods, see the solid red curve in Fig. 2(c). Moreover, it is noticeable that the 35% of energy that is not decoupled from the W1 waveguide is mostly transmitted. We have evaluated the ultimate potential of our structure by calculating the reflection for a semi-infinite coupler with $N = \infty$, see Fig. 2(d). In this case, $T = 0$ and all the energy that is not

reflected can be extracted by the coupler, $O = 1 - R$. Quite surprisingly, for large group indices $40 < n_g < 100$, the W1 waveguide mode is only poorly reflected, $R < 20\%$, and the extraction efficiency is large, $O > 80\%$ [see also Fig. 5(b)]. Note also that the Fabry-Perot fringes outside the band-gap disappear for a semi-infinite coupler.

In Section 3, we demonstrate experimentally the feasibility of the design by coupling slow light in and out of a W1 waveguide made in an InP membrane over a large group-index range, $10 < n_g < 60$. Then, in Section 4, we further analyze numerically the potential of the proposed structure by studying the impact on the coupler performance of geometrical parameters such as the period $a_c$ and the perturbation $\Delta r$.

## 3. Experimental results

As a proof of principle for the proposed geometry, we fabricated and tested an InP based system composed of two couplers separated by a 200-µm-long W1 waveguide. Light is coupled into the sample by illuminating one coupler and we measure the fraction of light that is extracted with the second coupler after propagation in the 200-µm-long waveguide. We demonstrate that light has really propagated in the W1 waveguide by retrieving its group-index evolution directly from the measured transmission spectrum.
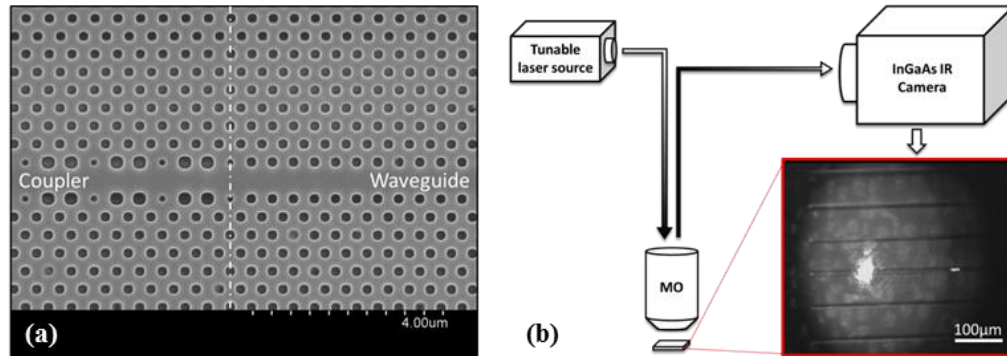


Fig. 3. (a) SEM picture of the interface between the W1 waveguide (on the right of the dashed-dotted white line) and the heterostructure coupler (on the left of the dashed-dotted white line). (b) Simplified description of the transmission measurement setup. The red framed picture shows different parallel waveguides (horizontal dark lines) with light being coupled into the central one. The large bright spot on the left is the incident spot reflected by the input coupler and the weak elongated spot on the right correspond to the output coupler and shows where the light is extracted from the waveguide.

The waveguide-coupler system is made on a suspended InP membrane (265 nm thick) grown by MetallOrganic Chemical Vapor Deposition (MOCVD). A 1µm $SiO_2$ sacrificial layer underneath the InP is bonded on a Si substrate through a BenzoCycloButene (BCB) layer [28] and the air spacer is obtained after etching this sacrificial layer. The W1 waveguide is generated by introducing a line defect (one missing row of holes) in a PhC triangular lattice with a period of $a = 440$ nm and with holes of radius $r = 120$ nm. Based on the design described in Section 2, two couplers are introduced in this line defect at a 200 µm distance from each other with the following parameters, $\Lambda = 3a_c$, $a_c = a + 30 = 470$ nm, $\Delta r = 35$ nm. The coupler length is set to be $L_c = 15\Lambda$ which corresponds to a physical length of $L_c = 21.15$ µm. Figure 3(a) presents a Scanning Electron Microscope (SEM) picture of the junction (dashed-dotted white line) between the waveguide and the coupler.

A simplified description of the setup used to measure the transmission is described in Fig. 3(b). A fibered continuous-wave (cw) laser tunable from 1490 nm to 1650 nm is coupled in the W1 waveguide via a 10X microscope objective (0.25 NA) and a high sensitivity InGaAs infrared camera images the whole {coupler – waveguide – coupler} system. The red framed picture presents a camera image of a sample in a transmission measurement configuration.

Several waveguides appear horizontally on the image with only one in the center of the image being coupled in and out. The brightest spot is the reflection of the injection signal around the input coupler while the small and elongated spot corresponds to the decoupled signal from the output coupler after propagation through the 200-µm-long PhCW. The transmitted signal is then isolated by spatially filtering it on the image and transmission measurements are achieved by integrating the pixel intensity in this selected part of the image for each wavelength of the tunable laser sweep.

Figure 4(a) shows a typical measured transmission spectrum corresponding to the W1 waveguide previously described in this section. As shown in Fig. 2, the reflection R of the W1/coupler interface can be large (particularly in the band-gap) and Fabry-Perot fringes thus appear in the transmission spectrum. The high wavelength limit in the transmission spectrum is set by the cut-off of the W1 waveguide; this spectral range corresponds to very large group index values that are linked to strong disorder-induced losses and low transmission values for the whole system [18,29]. For low wavelength values the transmitted signal does not exhibit Fabry-Perot fringes since the drop of the coupler reflectivity induces their extinction. Still, the extraction efficiency of the coupler in this spectral range is not zero and the transmitted signal does not vanish and remains above the noise level.
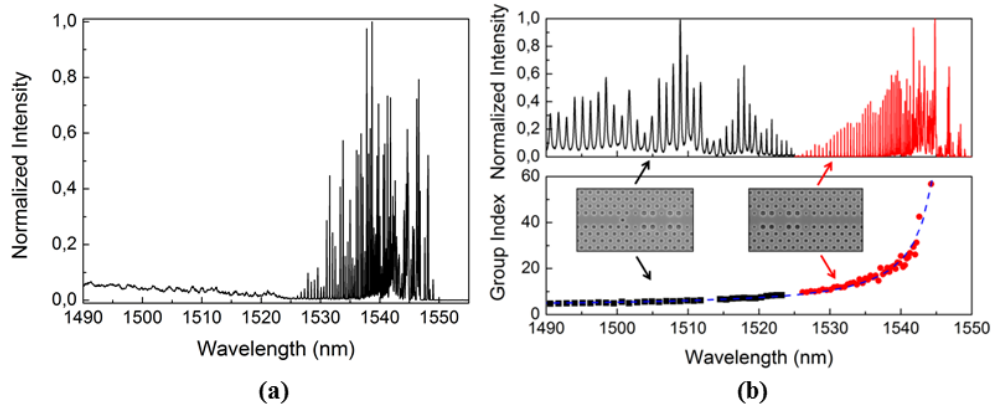


Fig. 4. (a) Normalized intensity of a typical transmission signal measured for a 200-µm-long system {coupler - W1 – coupler}. (b) Top part: Black and red lines represent the transmitted signal of two different systems put end-to-end. The red line corresponds to the same system as in (a), while the black line corresponds to a system with one additional hole in the waveguide at the W1/coupler junction (see the SEM picture in the inset). Bottom part: Black dots and red dots represent the group-index values respectively extracted from the corresponding measured transmission signal. In addition, the blue dashed line presents a numerical calculation of the group index evolution. The insets present SEM pictures of the actual coupler region respectively with and without the "mirror hole".

By exploiting the Fabry-Perot fringes, it is possible to retrieve the group delay that is due to light propagation inside the waveguide between both couplers and consequently to determine the group index of the W1 waveguide. Indeed, the group index $n_g$ associated to light propagation inside the sample is given by the free spectral range (FSR) of the Fabry-Perot resonances [1,30]

$$n_g = \frac{\lambda^2}{2L\Delta\lambda} \qquad (2)$$

where $\Delta\lambda$ is the Free Spectral Range (FSR) and $L = 200$ µm is the length of the waveguide. In this configuration, the frequency-dependence of the reflection phase at the W1/coupler interface negligibly impacts the FSR [29]. This has been confirmed from computational results for the modal reflection based on the actual PhCW parameters showing a group index

variation of less than 5% for reasonable group index values. Above these group index values disorder-induced effects have a strong influence on the experimental determination of the group index that exhibits a significant dispersion, which is largely predominant in comparison with any other effect.

The top part of Fig. 4(b) presents two measured transmitted signal (black line and red line) corresponding to two distinct systems {coupler - W1 – coupler} with strictly identical parameters except for one single hole inserted at each junction W1/coupler and acting as a mirror for low wavelength values. Indeed, as it has already been presented by Mazoyer in [29], this hole drastically enhances the reflectivity and therefore induces a Fabry-Perot fringes apparition. In the end, by superimposing both measurements it is possible to retrieve group-index values for the whole spectral area of the transmitted signal. The bottom part of Fig. 4(b) presents the group-index values respectively extracted from the corresponding transmission measurements (black dots and red dots corresponding to black line and red line) while the blue dashed line represents computational data of the group-index evolution (a spectral offset was added to take into account the difference between the targeted and actual technological parameters) obtained by a calculation based on the actual parameters of the W1 waveguide. Both experimental and computational data show a very good agreement. It demonstrates that slow light has been coupled in the PhCW, has propagated over 200 µm and has been extracted by the second coupler over a broad group index range $10 < n_g < 60$.

To complete these measurements the powers impinging onto the input coupler and coming out of the output coupler were measured to estimate a transmission value for the whole system {coupler + W1 + coupler}. From the transmission, we have tried to deduce the coupling efficiency. The measured input power value was corrected to take into account the area mismatch between the coupler and the injection spot, a Gaussian spot of 5 µm waist leading to an area overlap of 10%. The transmission was measured both in non-slow-light regime ($n_g = 5$) at 1500 nm and in slow-light regime ($n_g = 30$ on a transmission peak) at 1542.8 nm. These measurements led respectively to transmission values of 0.02 ‰ in the first case and 0.3 ‰ in the second one.

The coupling efficiency of the coupler was then deduced by assuming that the total transmission is given by the product of three quantities: the coupling efficiency, the transmission of the W1 and the extraction efficiency. Assuming the W1 transmission to be equal to 1 (no losses) we separated two different cases: Firstly at 1500 nm where the extraction efficiency was assumed to be equivalent to the previously calculated out-of-plane losses (see Fig. 2) and secondly at 1542.8 nm where the extraction efficiency was obtained from a Fabry-Perot formula based on the calculated parameters. Consequently, with extraction efficiencies of respectively 5% and 40% (and a factor of 2 accounting for the vertical symmetry of the calculated system) the coupling efficiency was determined to be 1 ‰ and 2 ‰ respectively at 1500 nm and 1542.8 nm.

These values show the same order of magnitude for the coupling efficiency whether with or without Fabry-Perot fringes in the transmission (respectively in slow-light and non-slow-light regime). They also appear to be low in comparison with state-of-the-art values however one must consider that they are only under-estimations of the actual ones. Indeed several potential origins of losses such as the use for this measurement of a confocal detection system (imaging the output coupler on a fiber) or the losses associated to the slow-light propagation were not taken into account. Furthermore, aside from the main emission angle, the full radiation pattern still remains to be investigated in detail in order to be matched best to the incident field. In conclusion, beyond this first experimental proof of concept we believe that a systematic study will allow a better understanding of the coupling mechanisms and significant improvements of their efficiency.

## 4. Impact of various geometrical parameters

The structure proposed in Section 2 and characterized in Section 3 allows efficient coupling and extraction of slow light in a PhCW. In this Section, we study numerically the impact on the performance of some geometrical parameters such as the period $a_c$ and the perturbation $\Delta r$.

Starting from the structure designed in Section 2 ($a = 430$ nm, $a_c = 460$ nm, $\Delta r = 35$ nm, $N = 30$), we vary the longitudinal period $a_c$ in the coupler. The results are presented in Fig. 5 as a function of the group index of the incident W1 waveguide. Figure 5(a) shows the variation of the extraction angle $\theta = \arcsin[\mathrm{Re}(n_{\mathrm{eff}}) - m\lambda/\Lambda]$, with $n_{\mathrm{eff}}$ the effective index of the coupler Bloch mode, for $a_c = 450, 460, 470, 480$ and $490$ nm (magenta, red, black, green and blue curves respectively). The group index values for which $\theta \approx 0$ corresponds to the band-gap of the leaky Bloch mode at $k = 0$ [see Fig. 2(b)]. For $a_c = 460$ nm, the band-gap lies around $n_g = 20$. The main effect of the period variation is to shift the band-gap position: an increase of the period $a_c$ shifts the band-gap towards larger group indices. Indeed, for $a_c = 450$ nm, the band-gap is below $n_g = 10$ [magenta curve in Fig. 5(a)] and for $a_c = 470$ nm, the band-gap edge has been shifted to $n_g \approx 70$ [blue curve in Fig. 5(a)]. For larger periods, $a_c = 480$ and $490$ nm, the band-gap fully lies below the W1 waveguide cut-off at wavelengths larger than $\lambda_g = 1.561$ μm. The immediate consequence of the band-gap red shift is the increase of the wavevector and hence the increase of the extraction angle, as evidenced in Fig. 5(a). For the periods under study, the extraction angle remains below $\pm 15°$, which corresponds to small numerical apertures (N.A. $< 0.26$).
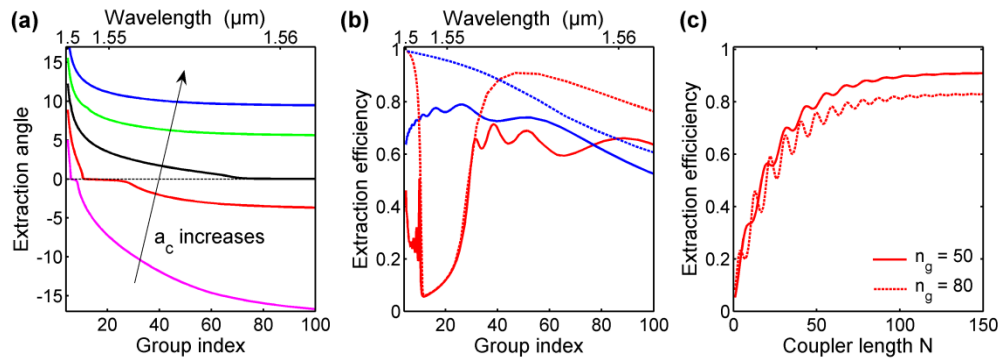


Fig. 5. Performance of the coupler for different values of the longitudinal period $a_c$. The other geometrical parameters of the system are the same as in Fig. 1(d) with $\Delta r = 35$ nm. (a) Extraction angle $\theta$ for $a_c = 450, 460, 470, 480$ and $490$ nm (magenta, red, black, green and blue curves respectively). (b) Extraction efficiency $O = 1 - R - T$ for $a_c = 460$ nm (red) and $a_c = 490$ nm (blue). Solid and dashed curves correspond to $N = 30$ and $N = \infty$ (semi-infinite coupler). (c) Extraction efficiency as a function of the coupler length for $a_c = 460$ nm. $N$ is the number of super-periods in the coupler, $L_c = N\Lambda$, see Fig. 2(a). Solid and dashed curves correspond to $n_g = 50$ and $n_g = 80$.

Shifting the band-gap position allows us to tune the group-index range where the extraction efficiency is high. Figure 5(b) shows the extraction efficiency of finite-size ($N = 30$) and semi-infinite couplers ($N = \infty$) for $a_c = 460$ nm (red) and $a_c = 490$ nm (blue). For the latter case, the band-gap is completely shifted outside the spectral range of interest and the extraction efficiency is large ($O > 60\%$) over the whole group-index range, from fast ($n_g = 5$) to very slow light ($n_g = 100$), see the solid blue curve in Fig. 5(b). By increasing the coupler length (as shown in Fig. 5(c)), higher efficiencies can be reached over a group-index range that depends on the period. For $a_c = 460$ nm, the group-index range where the extraction efficiency exceeds 80% is $40 < n_g < 100$ while for $a_c = 490$ nm it is blue-shifted to $10 < n_g < 60$.

In a second step we have studied the effect of a variation of the perturbation $\Delta r$. The main impact is also a shift of the band-gap position and hence of the group-index range where the extraction efficiency is high. We have performed numerical calculations (not shown here) which evidence that an increase of $\Delta r$ induces a blue shift of the band-gap position. For similar relative changes, the spectral shift induced by a variation of $\Delta r$ is smaller than the one induced by a variation of the period $a_c$.

Finally, we have analyzed the variation of the extraction efficiency with the coupler length. We have calculated the extraction efficiency $O = 1 - R - T$ as a function of the number $N$ of super-periods [$L_c = N\Lambda$ as defined in Fig. 2(a)] for $n_g = 50$ and $n_g = 80$. Whatever the group-index value, the impact of the length is the same: the two-third of the maximum extraction efficiency is reached for $N = 30$ super-periods ($L_c \approx 40$ µm) and 70 super-periods are necessary to achieve 95% of the maximum extraction.

## 5. Conclusion

We demonstrated the extension of the band-folding procedure to PhC waveguides and the generation of couplers able to couple light in and out W1 waveguides operating in the slow-light regime over a broad group-index range from 10 to 60. We also showed numerically that slow light ($50 < n_g < 100$) from the W1 waveguide can be very efficiently injected (insertion loss below 10%) into the fundamental Bloch mode of the coupler and then extracted out of the waveguide at nearly normal incidence ($|\theta| < 5°$). The designed devices was fabricated with InP-based W1 suspended PhCWs and transmission measurements over a 50 nm bandwidth confirmed the possibility of coupling and extracting slow light at normal incidence in good agreement with theoretical predictions. Beyond this proof of principle we discussed the influence of the critical parameters of the coupler over its performances and showed that a careful engineering of the coupler allows us to achieve simultaneously high extraction efficiency and low facet reflectivity at a selected spectral range corresponding to $n_g$ values of a few tens.